Pergamon

Scripta Materialia, Vol. 39, No. 12, pp. 1705–1712, 1998
Elsevier Science Ltd

1359-6462/98 $19.00 + .00

PII S1359-6462(98)00385-6

MAPPING TWO-DIMENSIONAL STATE OF STRAIN USING SYNCHROTON X-RAY DIFFRACTION

Alexander M. Korsunsky[†], Karen E. Wells[†] and Philip J. Withers[‡]
[†]Department of Mechanical, Materials and Manufacturing Engineering, Materials Division, University of Newcastle, Newcastle upon Tyne, NE1 7RU, UK [‡]Department of Materials Science and Metallurgy, University of Cambridge, Pembroke Street, Cambridge, CB2 3QZ, UK

(Received February 16, 1998)
(Accepted in revised form September 14, 1998)

Introduction

Composite strain mapping is a procedure which is naturally addressed by techniques utilising diffraction. Measurements in both the matrix and reinforcement cannot be made using conventional methods, such as strain gauging or hole drilling. Diffraction techniques most commonly used for strain measurements include neutron diffraction, conventional (laboratory) X-ray, and synchrotron X-ray diffraction. Compared to laboratory X-ray, synchrotron radiation offers dramatic improvements in beam intensity and penetration depths. Where conventional diffraction stress measurements rely on interrogating only a thin surface layer ($<50\mu$m) of such material as aluminium, synchrotron X-ray possesses sufficient flux to allow collection of diffraction patterns from sampling volumes over 20mm thick. Important additional benefits of using such high flux beams are the improved spatial resolution, and the possibility of using extremely short collection times. These two experimental parameters are interrelated, and both influence the quality of data in a complex way. Additionally, acceptable data quality varies depending on the interpretation procedures and the requirements of accuracy and consistency. As a consequence, suitable values of the test parameters, such as sampling volume and collection time, must be determined experimentally, using carefully selected test systems, possessing suitable geometry and subjected to controlled loading. The main content of the present paper is the description of such an experiment.

In this study, measurements were made on the ID11, BL2 materials science beamline (1) at the European Synchrotron Radiation Facility at Grenoble, a diffractometer allowing controlled translation of the sample in three linear directions. The technique involved direct collection of diffracted patterns in digital form using a high resolution CCD camera. Due to the novel nature of this application, the capabilities and limitations of the present configuration for engineering strain measurement had not yet been fully explored in a systematic way. The aim of the present experiment was to test the capabilities of both the hardware and software for making accurate and reliable strain measurements in the transmission geometry, to investigate their limitations, and to determine the routes for further development.

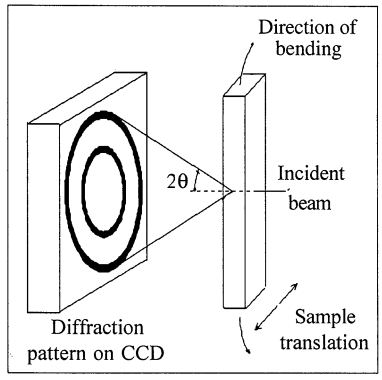

Figure 1. The experimental setup used at ID11, BL2 at ESRF.

Experimental Method

Test samples chosen for this experiment were 14 × 14 × 95mm smooth surface bars machined out of a metal matrix composite plate produced by a powder metallurgy route. The composite consisted of Al2124 alloy matrix reinforced with 17vol% SiC particles, which had the average diameter of 3μm. The composite plate was subjected to solution heat treatment appropriate for the base alloy, followed by quenching into cold water.

Quenching results in a state of residual macrostress which has been studied in some detail both experimentally and theoretically (2,3), due to its remarkable simplicity. The stress variation through the plate thickness is represented by a parabola, which must be symmetric with respect to the plate centre. The requirement of stress balance imposes an additional restriction on this profile, so that it can be characterised by a single parameter, such as the stress value at the plate surface, or at its centre σ_q. The difference in the thermal expansivity between the two phases results in the phase-average stress (and strain) 'splitting' (4,5). To the first approximation, these macroscopic thermal mismatch strains can be assumed uniform, and can be characterised by a single parameter, such as the effective temperature drop ΔT.

Machining of the bar specimen from quenched plate results in a partial relief, mainly of the macroscopic component of the residual stress pattern. Importantly, the deformed state observed within the plate cross section no longer corresponds to *plane strain*, although this approximation may be expected to remain valid for the points away from the specimen surface. The *plane stress* approximation provides a better description of the near surface region. The experimentally measured state of strain then represents a superposition of the plane strain-plane stress transition across the specimen thickness.

The bar specimens were subjected to four-point bending using an in-situ loading rig. Pure bending to moderate moment induces an elastic strain variation, which is superimposed on the residual strain. The elastic stresses and strains are partitioned between the phases in a way which is well modelled using such methods as the self-similar Eshelby ellipsoidal inclusion technique (6). The onset of plasticity first occurs on the compressive side of the bending specimen. It is aided by the macroresidual stress, which also leads to the asymmetry in tensile-compressive yielding behaviour, and in the extent of the corresponding plastic zones. These phenomena were successfully described using a mainly analytical method (4), which provides a convenient reference model. Measurements were made on the specimens loaded to two different degrees of plastic bending, and also subsequently to the removal of loading.

The X-ray diffraction experimental setup is illustrated in Figure 1. Specimens were mounted and translated in the plane normal to the beam. Beam collimation was used to define the sampling volume

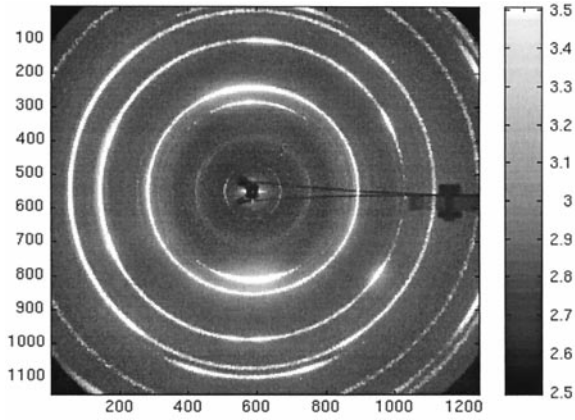

Figure 2. A diffraction pattern recorded by the CCD. The intensity scale shown is logarithmic base 10.

which had a shape of a square-based prism, elongated in the beam direction. This sampling geometry used allowed excellent spatial resolution in the lateral direction, with the spot size on the sample of 0.1×0.1mm. No longitudinal collimation was used in this present experiment presents a difficult experimental problem, which is presently being addressed by several research groups around the world, using specially designed conical collimating slits.

The photon energy used was 80keV, corresponding to the wavelength of approximately 0.155Å. Diffraction on a fine grained polycrystalline sample results in a family of cones, with the characteristic scattering angles of a few degrees for low order Al reflections. The ring-like patterns produced on a plane normal to the incident beam were acquired using an X-ray image intensifier, a Princeton CCD camera, providing 16-bit intensity readings over an array of 1242×1152 pixels. The number of complete diffraction rings collected from different phases could be varied by choosing the appropriate distance between the sample and the CCD camera. Figure 2 shows an example of the diffraction pattern recorded by the CCD.

Sample strain results in the distortion of the ideal circular pattern into an ellipse. This fact suggests the idea of using the complete ring pattern as the data set to be fit with an ellipse described by the three parameters: the major and minor semiaxes, and the orientation angle. Unfortunately, experience demonstrated unequivocally that the shape of the rings is dominated by the distortion effects, associated with the surface shape and pixel size variation of the CCD camera. This distortion was found to be too large to allow efficient correction for the present purposes, when reliable strain values need to be extracted with the accuracy of $<100\mu$strain.

Algorithm for Strain Evaluation

An alternative approach was adopted to the problem of determining the complete two dimensional strain state from the diffraction pattern.

Instead of attempting to fit the complete ring, lateral strain in any chosen direction was evaluated by considering the *radial displacement* of the peak centre with respect to a certain reference position. The implementation of the algorithm consists of the following steps:

(i) Find the pattern centre, which may not necessarily be identical with the position of the transmitted beam, due to the possible effects of distortion and deflection;

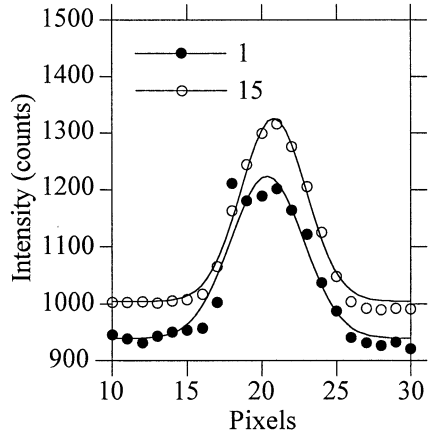

Figure 3. An example of the quality of the Gaussian fit and the difference between the angular averaging widths of 1° and 15°.

(ii) Perform *polar re-binning* of pixel intensity data into radius/angle bins with respect to the pattern centre;
(iii) Set polar angle width to be considered, sum the data over the polar angle onto a single line, and obtain a linear array of cumulative intensity values per radial position;
(iv) Perform Gaussian peak fitting of the two diametrically opposite peaks for each chosen strain direction;
(v) Evaluate strain using the formula

$$\epsilon = (D_0\text{-}D)/D_0,$$

where D_0 and D denote the *reference* and the *strained* ring diameters respectively (sums of radial peak positions at opposite angles).

It was established in the course of analysis that using the ring diameter, rather than its radius, for strain evaluation, ensures that the results are not particularly sensitive to the choice of pattern centre. Step (i) can be accomplished with sufficient accuracy by calculating the position of the mass centre for the chosen ring, followed by some refinement if necessary.

The polar re-binning step was the most time consuming, involving operations on approximately 1.5 million pixels per image. While the rest of the algorithm could be implemented using commercial data processing languages, such as IDL® or Matlab®, polar re-binning was performed by a separate C program written for the purpose, in order to achieve sufficient processing speeds of several seconds per data file on a PC. Radial intensity compensation was also applied by dividing the intensity calculated for each new bin by the number of points accepted. The result was written to a binary file in the form of radial intensity profiles on the segment between the radial positions of $r_{\min}$ and $r_{\max}$.

The re-binned files can be loaded into a data processing package for further analysis. Some variety of peak fitting routine is required in order to determine the radial position of the peak centre. However, attempts at fitting the data for each 1° bin directly often caused the fitting routines to fail. The reason for this is the scatter present in the data, as shown in Figure 3. It was found that averaging of the data over an angular range of 15° produced very smooth profiles, which could be easily and reliably fit by a single Gaussian curve with a flat background. An example of the resulting data and the corresponding fit quality is also illustrated in Figure 3. The choice of 15° angular averaging width is not expected to introduce significant error into the results.

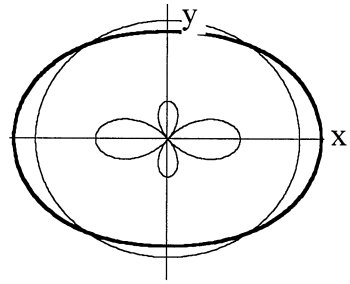

Figure 4. An illustration of bi-axial strain state. The unit circle (thin line) is distorted into the ellipse (thick line) by the application of principal strains ϵ_x and ϵ_y. The strain polar plot (inner contour) is obtained from the difference between the ellipse and the circle.

In an earlier publication (7), the use of a similar experimental set-up on BL2, ID11 at ESRF for strain measurement is described. However, in that case only relatively narrow horizontal and vertical strips were extracted from the CCD camera image. Strain evaluation was limited to those two directions, and carried out by collapsing the data onto a single linear profile. The method adopted in this study has the advantage of minimising peak smearing due to ascribing incorrect radial positions. It also allows strain evaluation in any orientation, making it possible to determine the principal strain values and directions.

The angular variation of strain can be visualised using a strain polar plot. Figure 4 illustrates the point that strain values are derived from the difference between the *deformed* shape (ellipse), and the *reference* shape (circle). As a result, lateral strain values may be positive in some directions and negative in others, producing loops of the kind shown in the picture. Shear strains produce a distortion which is a combination of rotation and stretching. Figure 5 gives an example of an experimentally measured strain polar plot (markers), with the solid line giving a fit. Good alignment of the figure with the co-ordinate axes shows that they also correspond to the principal strain directions.

Results and Discussion

The use of fine grained composite samples produced good peak intensities (~1500 counts, background ~1000 counts) using fairly fast acquisition times of less than 30 seconds per image. The beam spot size used was $100 \times 100\mu$m, allowing the best spatial resolution of 0.1mm. It was verified that the spot size

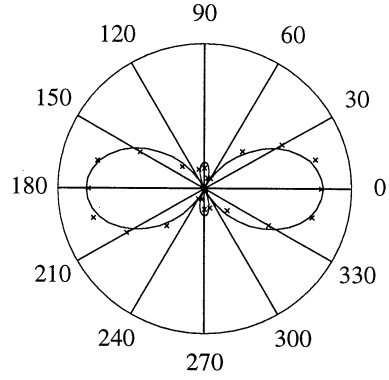

Figure 5. A strain polar plot representing the strain in the matrix in the loaded condition. The continuous curve shows a fit to the experimental data points (markers).

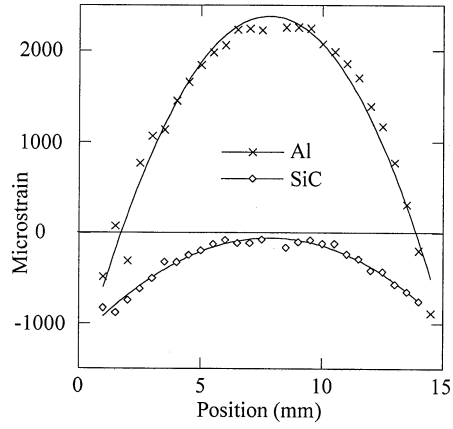

Figure 6. The variation of strain with position in the reference condition.

could be reduced further down to $10 \times 10\mu$m, still yielding interpretable measurements, although increasing graininess of the diffraction pattern was apparent. It is clear that further development of the analysis algorithm would be required, if speckly diffraction patterns were to be used for strain measurement.

The specimen was scanned in steps of 0.5mm. The strains were determined in steps of 15 degrees using Al (200) and SiC(111) reflections. The Al(111) ring which was incomplete due to the texture of the sample was not used. The results show very good consistency in the measurements made at adjacent positions (Figures 6, 7).

In any diffraction strain measurement study it is necessary to be able to assess, and if possible to minimise the measurement error. However, it is also important to distinguish between various causes producing diffraction peak shifts, and associated strain variations. Depending on the desired interpretation, various approaches can be adopted.

In the present study we focused on mapping the strain variation as a function of position in the specimens and the azimuthal angle; no attempt was made to determine the exact lattice spacings to the highest possible accuracy. This allowed us to disregard such sources of error as inaccuracies in

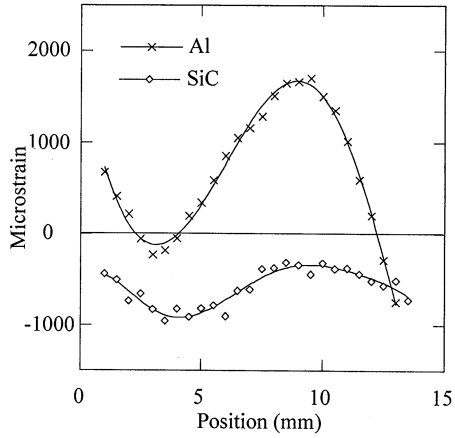

Figure 7. The variation of strain with position in the sample unloaded after plastic deformation.

positioning the sample and in determining the distance to the detector. Instead, it was assumed that a certain diffraction pattern could be chosen as reference, and strain values were computed from peak shifts relative to this reference. In view of the small diffraction angles used, errors in the choice of 'strain free' pattern contribute solely to shifts of the entire strain profile with respect to the zero strain level.

The error could therefore be estimated from the statistical analysis of the curve fitting process. The fit accuracy was improved by the binning procedure, and led to the estimated errors for determining the strain variation of 50 μstrain in the matrix and 100 μstrain in the reinforcement.

It is interesting to note that the knowledge of the mechanical state of the specimens being studied is useful in providing a rough test of how well the reference pattern was chosen. In particular, the thermal property mismatch between the phases leads to a difference in the average phase strain. Its value in the present study agrees with the results for the same specimen series obtained by alternative techniques, such as neutron diffraction. Furthermore, the results indicate that the requirement of macroscopic stress balance across the specimen section is satisfied.

The measured longitudinal strain profile is shown in Figure 6. The profiles show good smoothness and symmetry, with only the measurements taken at points near the edge of the sample showing some scatter, probably due to partial emergence of the sampling volume through the surface. The characteristic macroscopic residual strain profile due to quenching is clearly recognisable, with the measurements made in both phases showing excellent agreement with parabolic fits. A comparison with the results of neutron diffraction studies in similar materials (4) shows a significant improvement in the data quality. This applies to the values for the SiC reinforcement in particular. In terms of the average microscopic strain, as expected, the matrix finds itself in residual tension, compared with residual compression in the reinforcement.

Figure 7 shows the profile of the same strain component, measured in the plastically deformed sample in the unloaded condition. The smoothness of the data is once again apparent. In particular, such parameters as the location of profile minimum and maximum, gradients, elastic-plastic boundaries, etc. can be reliably extracted from the plots. This would allow quantitative modelling (e.g. (3)) to be applied in order to determine yielding and hardening properties of the composite material. In conjunction with suitable micromechanical modelling, the data can also be used in order to separate the residual stresses into macro- and various micro- components, and to elucidate the nature of residual stress evolution due to plasticity.

Conclusions

A novel approach has been described for the evaluation of the complete two dimensional elastic strain in polycrystalline samples using synchrotron X-ray diffraction and digital pattern collection and analysis. The developed procedure allows the complete angular strain variation, and hence the magnitudes and direction of the principal strains, to be determined from a single image, using collection times of less than 30 seconds, giving strain measurement accuracy of $\sim$50–100μstrain, and spatial resolution of 100μm.

Acknowledgments

The authors would like to thank Åke Kvick and Heinz Graafsma for their invaluable help in carrying out the measurements; ESRF for providing access to the facilities, and financial support through the EC TMR programme; and the University of Newcastle upon Tyne for funding through a Research Committee studentship.

References

1. A. M. Korsunsky, P. J. Withers, and P. J. Webster, ESRF Experiment Report HS300 (1997).
2. M. E. Fitzpatrick, P. J. Withers, and M. T. Hutchings, Acta Mater. 45, 4867 (1997).
3. A. M. Korsunsky and P. J. Withers, Int. J. Solids Struct. 34, 1985 (1997).
4. M. R. Watts, M. E. Fitzpatrick, A. M. Korsunsky, and P. J. Withers. in Proceedings of the 4th European Conference on Residual Stresses (ECRS 4), Cluny, France (1996).
5. I. C. Noyan and J. B. Cohen, Mater. Sci. Eng. 75, 179 (1985).
6. O. B. Pedersen, Acta Metall. 31, 1795 (1983).
7. M. R. Daymond and P. J. Withers. Scripta Mater. 35, 1229 (1996).